MATERIALE PLASTICE
https://revmaterialeplastice.ro
https://doi.org/10.37358/Mat.Plast.1964

Electrospun $LiFe_xMn_{1-x}PO_4$/C Composite Nanofibers for Lithium-Ion Batteries

OZAN TOPRAKCI*
Yalova University, Engineering Faculty, Department of Polymer Materials Engineering, Yalova, Turkey

Abstract. *Since the commercialization of Li-ion batteries by Sony in 1990, the performance of cathode materials used in Li-ion batteries has improved significantly. However, Li-ion batteries cannot respond to the needs of the energy storage market in terms of energy density. In order to increase theoretical energy density of active materials, molar mass of the active material should be decreased, or electron number participating per reaction or reaction potential should be increased. In this study, it was aimed to produce cathode materials for Li-ion batteries in the form of composite nanofibers via electrospinning method. For this purpose, porous $LiFe_xMn_{1-x}PO_4$/C composite nanofibers ($1 > x > 0$) were synthesized with a scalable, two-step method (electrospinning and subsequent heat treatment). The morphological, structural and electrochemical properties of the $LiFe_xMn_{1-x}PO_4$/C composite nanofibers were determined by scanning electron microscope, X-ray diffraction and galvanostatic charge/discharge tests. Cathodes made of $LiFe_xMn_{1-x}PO_4$/C composite nanofibers showed various advantages such as long cycle life, improved electrochemical performance etc. due to the presence of carbon and $LiFe_xMn_{1-x}PO_4$ in the composite structure. With the addition of Mn to the structure of $LiFePO_4$/C composite nanofibers, electrochemical performance was improved. $LiFe_{0.8}Mn_{0.2}PO_4$/C composite nanofibers showed the best performance in terms of energy density among the samples. Further increment in Mn/Fe ratio resulted declining electrochemical capacity and energy density.*

Keywords*: Binder-free electrodes, electrospinning, $LiFe_xMn_{1-x}PO_4$/C, Li-ion batteries*

1. Introduction

Lithium-ion batteries (LIBs) have become the common power sources in commercial applications such as portable electrical devices, electric vehicles and hybrid vehicles, parallel with the increased interest in lighter, thinner and smaller products [1]. Demand in high capacity and high voltage electrode materials is also increasing day by day for high energy applications. Among the cathode materials used in LIBs, lithium metal phosphates ($LiMPO_4$; M: Fe, Mn, Co) are one of the most promising materials due to their high capacity, high voltage and safety. Redox potentials for $LiMPO_4$ (M: Fe, Mn, Co, M^{+3}/M^{+2} vs. Li/Li^{+1}), are ~3.4, 4.1 and 4.8 V, respectively. Although their theoretical capacities are close to each other (approximately 170 mA*h g^{-1}), the redox reactions occur at different voltages, so theoretical energy density of $LiMnPO_4$ and $LiCoPO_4$ are 20 and 40 % higher than $LiFePO_4$, respectively [1, 2]. In addition, Fe and Mn are not toxic and they are relatively cheap because of their high abundance, so low-cost production is possible for commercial LIBs [3-5]. $LiMPO_4$ contains active transition metals suitable for redox reactions within the stable phosphate structure and demonstrate high lithium-ion mobility as well as high electrochemical and thermal stability. However, it has very low electrical conductivity. For this reason, $LiMPO_4$ should be embedded in a conductive matrix in order to be used effectively as a positive electrode in LIBs [5]. Yamada et al. have suggested that $LiFexMn_{1-x}PO_4$ has a higher energy density than $LiMPO_4$ and can achieve higher capacity level due to the increase in the amount of Mn. However, with the increase in Mn/Fe ratio the capacity decreased in the different $LiFe_xMn_{1-x}PO_4$ samples obtained by conventional methods. For this reason, it is very important to determine the appropriate Mn/Fe ratio [6,7]. In another study, by Zhou et al. synthesized $LiFe_{0.15}Mn_{0.85}PO_4$/C nanocomposite by using high-energy ball milling. Discharge capacity of 103 mAh g^{-1} was achieved at 1C [8]. The high-energy mixing method used in this study raises questions in terms of material homogeneity and energy costs [9]. The high-energy mixing method used in this study raises questions in terms of material homogeneity and energy costs [10]. Meligrana *et al.* produced $LiFe_xMn_{1-x}PO_4$/C ($0<x<1$) nanocomposites by using surfactant via hydrothermal synthesis method.

**email:ozan.toprakci@yalova.edu.tr*

As given in the study, with the increase in the Mn ratio in the composite, the volume of the unit cell increased and the $LiFe_{0.75}Mn_{0.25}PO_4$/C sample achieved a capacity of 68 mAh g^{-1} at 14C [11]. Wang *et al.* synthesized $LiFe_{0.25}Mn_{0.75}PO_4$ nanorods on reduced graphene oxide by solvothermal method and its discharge capacity was 107 mAh g^{-1} at 50C [12]. In another study, $LiFe_{0.5}Mn_{0.5}PO_4$/C nanocomposites were synthesized by solvothermal synthesis method. Similar to other studies, high capacity values have been achieved at high C-rates [13]. Although the electrochemical performance, thermal and chemical stability of materials obtained by these methods are good, the expensive and labor-intensive methods spark question marks in terms of scalability. On the other hand, electrospinning is a well-known method for mass production of pristine or composite nanofibers [14-16].

All the studies given above were carried out by traditional synthesis methods and there are very limited studies in which electrospinning method was used. In one of these studies, $LiFe_xMn_{1-x}PO_4$/C (x: 0, 0.25, 0.50, 0.75 and 1) was synthesized by using polyvinylpyrrolidone (PVP) as a polymeric matrix. Nanofibers with an average diameter of 220 nm were obtained after heat treatment. Approximately 100 mAh g^{-1} capacity value was observed at 4C for $LiFe_{0.5}Mn_{0.5}PO_4$/C composite nanofibers [17]. This study differs from previous studies in terms of polymeric matrix, Mn/Fe ratios and thermal processing conditions. In our study, polyacrylonitrile (PAN) was selected as a polymer matrix. As known, PAN is a polymer commonly used in the production of carbon fibers, carbon nanofibers and carbon nanofiber composites. In addition, it is a very suitable polymer for obtaining fibers with electrospinning method due to its high dielectric coefficient. Nanofibers obtained from PAN can be used as separators in LIBs, or can be converted into carbon nanofibers by applying suitable heat treatment, and these materials can be used as anodes in LIBs [18]. In addition, PAN can be used for preparation of Fe_2O_3/C [19], Si/C [20], SnO_2/C [21] composite nanofibers and can be used as anode materials in LIBs. Composite nanofibers such as $LiFePO_4$/C [22] and Li_2MnSiO_4/C [23] were produced with PAN polymer matrix and were used as cathode material in LIBs.

In this study, electrospun, porous $LiFe_xMn_{1-x}PO_4$/C composite nanofibers ($1 > x > 0$) were synthesized via two-step method. In the first step precursor filled PAN solutions were electrospun. In the second step synthesis of $LiFe_xMn_{1-x}PO_4$/C composite nanofibers was carried out by heat treatment. The morphological, structural and electrochemical properties of the $LiFe_xMn_{1-x}PO_4$/C composite nanofibers were determined based on Fe/Mn ratio. Scanning electron microscopy (SEM), x-ray diffraction analysis (XRD) and electrochemical characterization methods were used to understand the relationship between performance and morphology/structure of $LiFe_xMn_{1-x}PO_4$/C composite nanofibers.

2. Materials and methods

2.1. Preparation of $LiFe_xMn_{1-x}PO_{4p}$ precursor solutions

In order to prepare $LiFe_xMn_{1-x}PO_4$/DMF precursors, lithium acetate dihydrate ($CH_3COOLi{\cdot}2H_2O$, %99.95, Sigma), iron (II) acetate ($Fe(CH_3COO)_2$, %95, Sigma), manganese (II) acetate ($Mn(CH_3COO)_2$, >%99, Sigma), phosphoric acid (H_3PO_4) were dispersed in dimethylformamide (DMF, Merck) with stoichiometric ratios as shown in Table 1. All chemicals were used without further purification and were used after drying in a vacuum oven (Daihan Wisd) at 50℃ for 24h. The total solid material concentration in the solutions was 16 wt%.

Table 1. Stoichiometric ratios of chemicals used in the preparation of precursors

	Li Acetate	Fe Acetate	Mn Acetate	H_3PO_4	Fe/Mn Ratio
$LiFePO_4$	1	1.0	0	1	-
$LiFe_{0.8}Mn_{0.2}PO_4$	1	0.8	0.2	1	4.00
$LiFe_{0.6}Mn_{0.4}PO_4$	1	0.6	0.4	1	1.50
$LiFe_{0.4}Mn_{0.6}PO_4$	1	0.4	0.6	1	0.33
$LiFe_{0.2}Mn_{0.8}PO_4$	1	0.2	0.8	1	0.25
$LiMnPO_4$	1	0	1.0	1	-

2.2. Preparation of PAN solutions

PAN with an average molecular weight of 150 kg mol^{-1} was obtained from Merck. DMF (Merck) was used as a solvent. All chemicals were used without further purification. PAN was used after drying in a vacuum oven (Wisd, WOV-20, Daihan) at 40℃ for 24 h. 8 wt. % PAN containing solutions were prepared by magnetic stirring (Wisd, MSH-20A, Daihan) at room temperature for 24 h and $LiFe_xMn_{1-x}PO_4$ precursor solutions (Table 1) were incorporated into the PAN solutions.

LiFexMn1-xPO4/DMF precursors and PAN/DMF solutions were mixed 1:1 by weight and mixed by an ultrasonic mixer for 12 h in order to prepare the final electrospinning solutions. The concentration of PAN and $LiFexMn_{1-x}PO_4$ precursors were 4 and 8 wt. % respectively in the final spinning solutions. The solution concentrations used in this study and the parameters of the electrospinning process were based on our previous studies [18, 20, 21].

2.3. Production and characterization of $LiFe_xMn_{1-x}PO_4$ precursor/PAN nanocomposite fibers and $LiFe_xMn_{1-x}PO_4$ /C nanocomposite fibers

The parameters for the electrospinning process were determined based on our previous optimization studies and can be given as: 0.5 mL h^{-1} feed rate, 15 cm tip-to-collector distance, 15 kV potential difference, ~25°C and ~60% relative humidity. $LiFe_xMn_{1-x}PO_4$ /C nanocomposite fibers were obtained after $LiFe_xMn_{1-x}PO_4$ precursor/PAN nanocomposite fibers were exposed to heat treatment. Two-step heat treatment was performed. In the first step, known as stabilization, the linear structure of PAN was deteriorated and turned into a ladder-type structure [18, 20, 21]. This process was performed under air at 280°C for 5 h. The second step was carried out under Argon at 700°C for 18 h and in this stage polymer chains in the ladder-type structure were cross-connected to form graphene layers in the structure.

2.4. Morphological characterization

$LiFe_xMn_{1-x}PO_4$ precursor/PAN nanocomposite fibers and morphology of $LiFe_xMn_{1-x}PO_4$/C nanocomposite fibers were examined by scanning electron microscope (SEM). In this study the SEMoscope-Tabletop-SEM device was used at 20 kV. The samples were sputter coated 3-6 nm thick with Au/Pd alloy before examination.

2.5 X-ray diffraction (XRD) analysis

XRD was used for structural characterization of $LiFe_xMn_{1-x}PO_4$/C (x: 1, 0.8, 0.6, 0.4, 0.2 and 0) composite nanofibers. The measurements were carried out in PANanalytical Empyrean at Eskisehir Osmangazi University Central Research Laboratory Application and Research Center. Measurements were made using Cu Kα radiation (wavelength 1.5405 Å) at 0.05°s^{-1} scanning speed in the range of 0-45°.

2.6 Electrochemical characterization

For the electrochemical characterization, approximately 20 μm thick composite nanofiber mats were cut in circular form with a diameter of approximately 12 mm, dried under vacuum at 100°C for 24 h. CR2032 type half-cells were prepared in the glovebox under Argon atmosphere (H_2O≤1 ppm; O_2≤1ppm). Al was used as a current collector, Celgard 2400 was used as a separator and lithium metal was used as reference electrode. 1M $LiPF_6$ salt was dissolved in ethylene carbonate, ethyl methyl carbonate and dimethyl carbonate (1:1:1 v/v/v) and this solution was used as an electrolyte. $LiFe_xMn_{1-x}PO_4$/C composite nanofibers were used directly as positive electrodes in Li-ion half cells. Cycle performance was analyzed by charging and discharging over 50 cycles in the range of 2.5 – 4.2 V at 34 mA g^{-1} current density (C/5). Schematic representation of experimental procedure of this study was given in Figure 1.

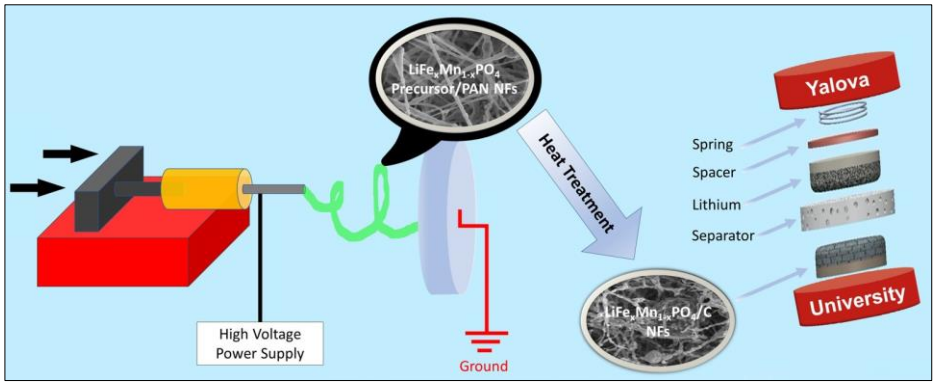

Figure 1. Schematical representation of experimental procedure

3. Results and discussions

3.1 Morphological characterization

In order to analyze the morphology of the electrospun fibers and fibers after carbonization process samples were analyzed by SEM. The electrospun fibers are shown in the first column in Figure 2 (a, e, i, m, r, v), in the second column in Figure 2 (b, f, j, n, s, w) carbonized nanofibers are given. The diameter distribution graphs of electrospun fibers (c, g, k, o, t, x) and carbonized fibers (d, h, l, p, u, y) are given in the third and fourth columns of Figure 2, respectively.

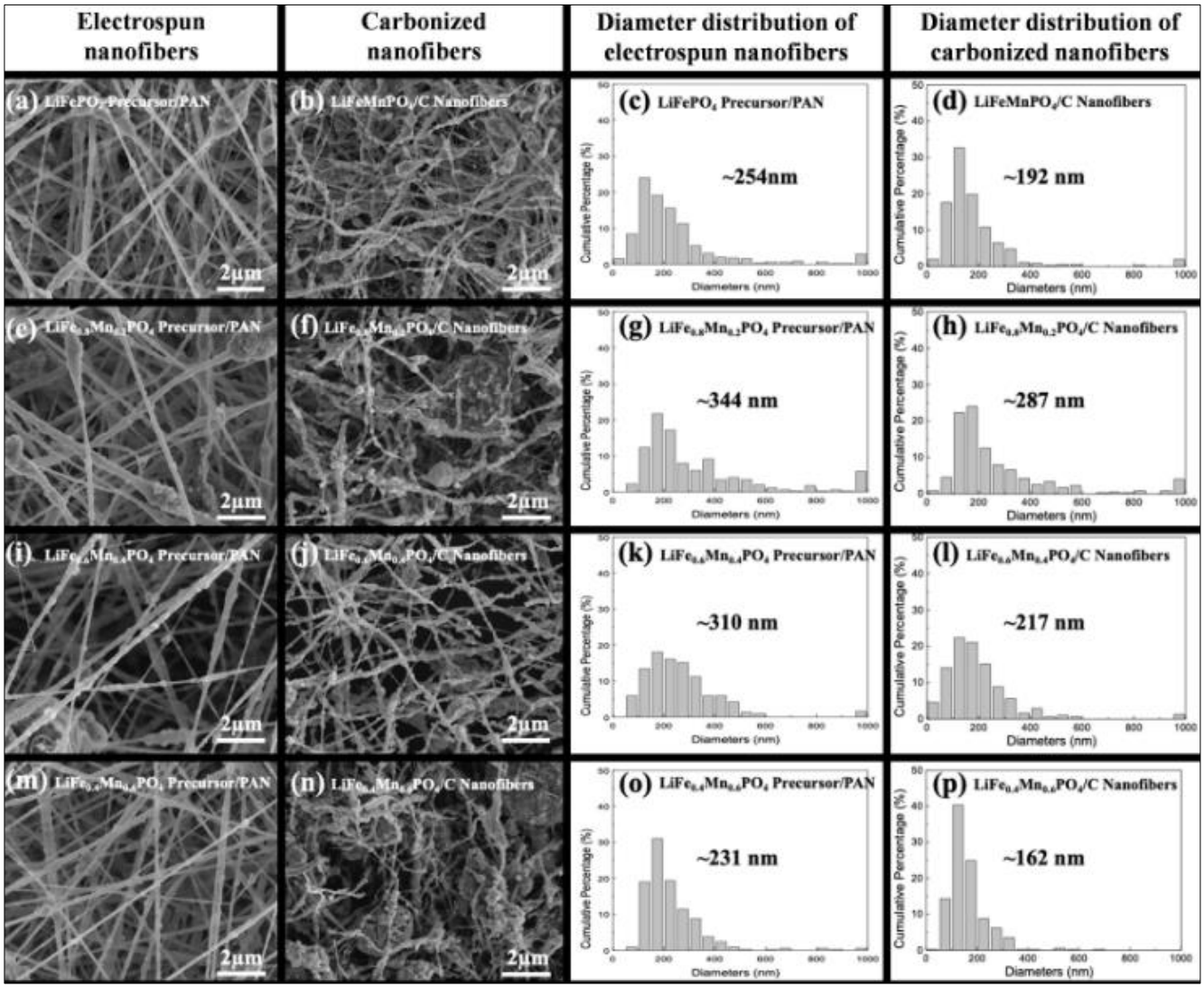

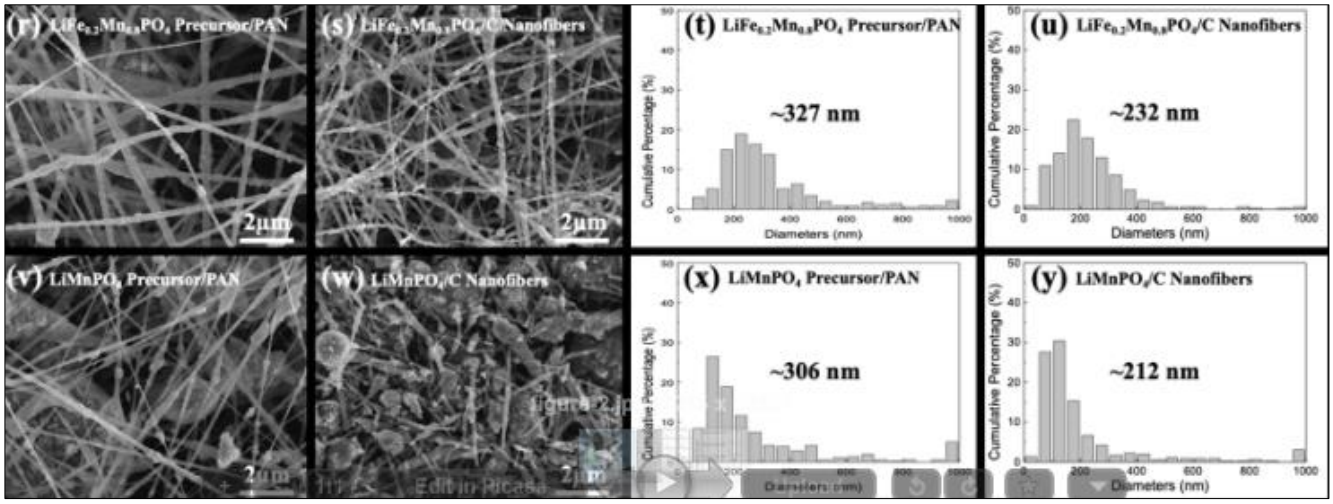

Figure 2. SEM images of electrospun fibers (a, e, i, m, r, v), carbonized nanofibers (b, f, j, n, s, w) the diameter distribution graphs of electrospun fibers (c, g, k, o, t, x) and carbonized fibers (d, h, l, p, u, y)

As can be seen from the first column of Figure 2 all samples were successfully electrospun with right-skewed diameter distribution. However, some irregularities such as agglomerations, bead formation were also observed in these samples due to high filler content. The average diameter of electrospun fibers nanofibers with the following precursors $LiFePO_4$, $LiFe_{0.8}Mn_{0.2}PO_4$, $LiFe_{0.6}Mn_{0.4}PO_4$, $LiFe_{0.4}Mn_{0.6}PO_4$, $LiFe_{0.2}Mn_{0.8}PO_4$, $LiMnPO_4$ were determined as 254, 344, 310, 231, 327, 306 nm, respectively.

As can be seen from images (Figure 2 a, e, i, m, r, v) precursors were homogeneously dispersed/embedded in the PAN matrix that is very critical for the synthesis and performance of the cathode materials. The average fiber diameter values for $LiFePO_4$/C, $LiFe_{0.8}Mn_{0.2}PO_4$/C, $LiFe_{0.6}Mn_{0.4}PO_4$/C, $LiFe_{0.4}Mn_{0.6}PO_4$/C, $LiFe_{0.2}Mn_{0.8}PO_4$/C, were calculated as 192, 287, 217, 162, 232, 212 nm respectively. As seen from images (Figure 2 b, f, j, n, s, w) active materials were nicely coated by carbon. After the carbonization process since PAN was converted into carbon, all fibers shrunk, and fiber diameter values decreased (Table 2) around 17-30%. It can be interpreted from SEM images, addition of Mn into the spinning solution, generally led to increase in the average fiber diameter compared to $LiFePO_4$ fibers. For $LiMnPO_4$/C at some places continuous fiber form was lost because of the agglomeration of the active materials. However, no direct relationship and significant difference were found between composition and fiber diameter for other Mn containing samples. That was also previously reported for $LiFe_xMn_{1-x}PO_4$/C composites synthesized by a solid-state route [26].

Table 2. Average fiber diameter, fiber diameter distribution and crystallite size values

	Before heat-treatment		After heat-treatment		
	$D^{\dagger}$ (nm)	FDU	$D^{\dagger}$ (nm)	FDU	$CS^{\ddagger}$ (nm)
$LiFePO_4$/C	254	1.72	192 (-24.4 %)	1.51	31.05
$LiFe_{0.8}Mn_{0.2}PO_4$/C	344	2.07	287 (-16.6 %)	2.01	36.42
$LiFe_{0.6}Mn_{0.4}PO_4$/C	310	1.36	217 (-30 %)	1.55	32.58
$LiFe_{0.4}Mn_{0.6}PO_4$/C	231	1.09	162 (-29.9 %)	1.16	29.07
$LiFe_{0.2}Mn_{0.8}PO_4$/C	327	1.60	232 (-29 %)	1.29	34.81
$LiMnPO_4$/C	306	2.64	212 (-30.7 %)	2.62	31.18

$D^{\dagger}$: average diameter; $CS^{\ddagger}$: crystallite size

In addition to fiber diameter distribution, fiber uniformity was also calculated. The following formula was used to determine the uniformity of the diameter distributions (FDU) of the fibers obtained before and after heat treatment:

$$FDU = \frac{D_{90} - D_{10}}{D_{50}} \quad (1)$$

Accordingly, D90, D50, D10 values correspond diameter value, which is 90%, 50% and 10% of the fibers, respectively. The closer the FDU value is to 1, the greater the uniformity of the diameter distribution [18]. Table 2 shows the change in the values of FDU for different samples before and after heat treatment. When Table 2 is examined, $LiFe_{0.4}Mn_{0.6}PO_4$ precursor/PAN and $LiFe_{0.4}Mn_{0.6}PO_4$/C were determined as the samples those showing the narrowest diameter distribution.

3.2 Structural characterization of $LiFe_xMn_{1-x}PO_4$/C nanocomposite fibers

XRD has been used for structural characterization of $LiFe_xMn_{1-x}PO_4$/C composite nanofibers. Scherrer equation was used to determine the average crystallite size (CS) of $LiFe_xMn_{1-x}PO_4$/C composite nanofibers [18]:

$$L = \frac{0.9 \times \lambda}{\beta \times cos\theta} \quad (2)$$

where λ is wavelength of the x-ray; θ is the Bragg angle; β is the half-height width of the peak and the K is the correction factor obtained at the end of XRD. The crystallite sizes of the 5 most pronounced peaks were calculated and the average of these values was taken in the calculation of the average crystallite size. Accordingly, characteristic peaks for $LiFe_xMn_{1-x}PO_4$/C composite nanofibers were observed at 35.59° (131), 25.56° (111), 29.70° (121), 20.77° (110) and 17.15° (020), respectively. Table 2 shows the average crystallite size and average diameter values for different samples after heat treatment. As a general trend, increase in the fiber diameter led to formation of bigger crystallites. That was probably caused by the higher probability of particle grow. In the case of higher diameter, the amount of precursor in the cross-section was assumed to be higher and that led to higher chance to formation of bigger particles. As obvious from the Figure 3, all samples matched with the olivine structure and no foreign crystal phases were observed. In parallel with the literature, as the Fe/Mn ratio increased XRD patterns appeared to shift to higher Bragg angles [8]. In addition to these results, Rietveld analysis with Highscore Plus software was also performed and, it was observed that all samples had orthorhombic crystal structure with *Pnmb* space group. Another observation related with the structure was small peak shift from 36° to 35° with the increase in the Mn content. That could be related to the lattice change from $LiFePO_4$ to $LiMnPO_4$ [26].

3.3 Electrochemical characterization of $LiFe_xMn_{1-x}PO_4$/C nanocomposite fibers

$LiFe_xMn_{1-x}PO_4$/C composite nanofibers were used directly as positive electrodes in Li-ion half cells. Cycle performance of the cathodes was analyzed by charging and discharging over 50 cycles in the range of 2.5 – 4.2 V at 34 mA g^{-1} current density (C/5). The cyclic performance results are given in Figure 4. Accordingly, $LiFePO_4$/C composite nanofibers showed the best cyclic performance. In general, as the Mn/Fe ratio in the $LMPO_4$/C (M: Fe, Mn) structure increased, the capacity value decreased. When the composite nanofibers were compared, $LiFe_{0.8}Mn_{0.2}PO_4$/C showed the most stable performance. The first cycle charge capacities for $LiFe_xMn_{1-x}PO_4$/C composite nanofibers with the value of x= 1, 0.8, 0.6, 0.4, 0.2 and 0 were found to be 140, 120, 100, 60, 60 and 6 mAh g^{-1}, respectively. Accordingly, the first cycle Coulombic efficiencies for $LiFe_xMn_{1-x}PO_4$/C composite nanofibers with the value of x= 1, 0.8, 0.6, 0.4, 0.2 and 0 were calculated as 82, 71, 62, 55, 55 and 12 %, respectively. With the addition of Mn into $LiFePO_4$, Coulombic efficiency decreased. There are basically two reasons for the decrease in electrochemical performance. One of them is the structural change given in XRD results. In the case of higher Mn/Fe ratio of LiFexMn1-xPO_4/C composite nanofibers, the shift was observed that was an indication of inherent lower electrical conductivity. The other reason can be given as the morphology of the active material. As can be seen from Figure 2, for $LiMnPO_4$/C at some places continuous fiber form was lost because of the agglomeration of the active materials. Since the connecting electrically conductive network formation was disturbed the electrochemical performance of $LiMnPO_4$/C was the lowest in all samples. The initial increase in capacity was thought to be due to the delayed penetration

of the electrolyte. As the electrolyte diffused into the porous structure over time, capacity values increased. However, these values are very inadequate for this sample to be commercialized. As noted by Yamada *et al.*, the Mn-rich phase ((1-x) > 0.8) in $LiFe_xMn_{1-x}PO_4$ is not suitable for high-specific capacity cathode materials. The strong electron–lattice interaction (Mn^{3+}: 3d4) in particular charged state ($(Fe_x^{3+}Mn_{1-x}^{3+})PO_4$) causes Jahn-Teller effect and limits the expansion and narrowing of the lattice, thus reducing the electrochemical activity [7, 8].

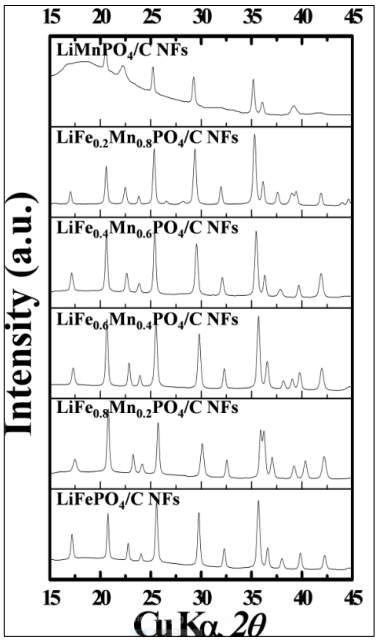

Figure 3. XRD patterns of $LiFe_xMn_{1-x}PO_4$/C composite nanofibers

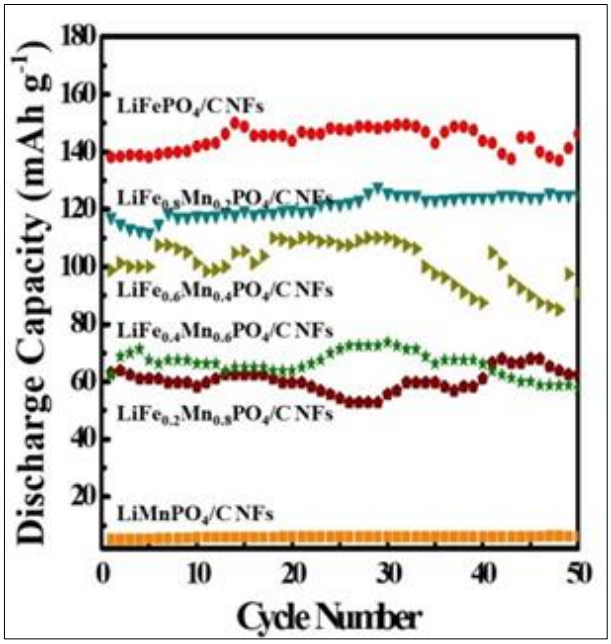

Figure 4. Cyclic performance of $LiFe_xMn_{1-x}PO_4$/C composite nanofiber based half-cells at

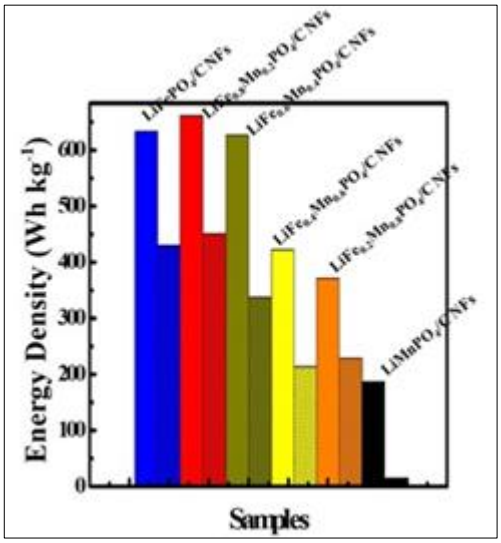

Figure 5. The first cycle energy densities of half cells produced from $LiFe_xMn_{1-x}PO_4$/C composite nanofibers

In Figure 5, the charge/discharge energy densities of $LiFe_xMn_{1-x}PO_4$/C composite nanofibers were evaluated. When Figure 5 was examined, the first cycle discharge energy densities obtained from $LiFe_xMn_{1-x}PO_4$/C composite nanofibers with the value of x: 1, 0.8, 0.6, 0.4, 0.2 and 0 were determined as approximately 430, 450, 337, 214, 229 and 15 Wh kg^{-1}, respectively. Accordingly, the highest energy density was obtained for $LiFe_{0.8}Mn_{0.2}PO_4$/C composite nanofibers during charging and discharging. When the Mn ratio in the $LiFe_xMn_{1-x}PO_4$/C structure was more than 0.2, significant reduction in capacity and energy density were observed.

4. Conclusions

In this study, $LiFe_xMn_{1-x}PO_4/C$ composite nanofibers were synthesized via combination of electrospinning and thermal process. PAN was used as the binder material for the precursors in the electrospinning solution and as the carbon source for the cathode material. The morphological, structural and electrochemical characteristics of the fibers were determined. Precursor containing nanofibers were successfully electrospun. $LiFe_xMn_{1-x}PO_4/C$ composite nanofibers showed lower average fiber diameter values compared to precursor filled samples. The structure of $LiFe_xMn_{1-x}PO_4/C$ composite nanofibers matched with the olivine structure and no foreign crystal phases were observed. As the Fe/Mn ratio increased, XRD patterns appeared to shift to higher Bragg angles and all samples had orthorhombic crystal structure with pnmb space group. The first cycle charge capacity values of $LiFe_xMn_{1-x}PO_4/C$ composite nanofibers with the value of x= 1, 0.8, 0.6, 0.4, 0.2 and 0 were determined as 140, 120, 100, 60, 60 and 6 mAh g^{-1}, respectively. The first cycle Coulombic efficiencies for $LiFe_xMn_{1-x}PO_4/C$ composite nanofibers with the value of x= 1, 0.8, 0.6, 0.4, 0.2 and 0 were determined as 82, 71, 62, 55, 55 and 12%, respectively. In general, the charge capacity and Columbic efficiencies decreased as the Mn/Fe ratio in the composite nanofiber structure increased. Among all composite nanofiber samples, $LiFe_{0.8}Mn_{0.2}PO_4/C$ showed the most stable performance with the highest energy density.

Acknowledgments: This study was funded by Yalova University. BAP (Scientific Research Project) Project No: 2015/BAP/118.

References

1.ZUBIZARRETA, L., GIL-AGUSTI, M., ESPINOSA, J.C., GARCÍA-PELLICER, M., QUIJANO-LÓPEZ, A., Studying the Properties of PVdF-HFP Based Lithium Polymer Electrolytes Using non-ionic Surfactants as Plasticizers, *Mater. Plast.*, **58**(1), 2021, 237-247 DOI: 10.37358/mp.21.1.5463.
2.ARAVINDAN, V., GNANARAJ, J., LEE, Y.-S., MADHAVI, S., $LiMnPO_4$ – A next generation cathode material for lithium-ion batteries, Journal of Materials Chemistry A, **1**(11), 2013, 3518-3539 DOI: 10.1039/C2TA01393B.
3.LI, G., AZUMA, H., TOHDA, M., Optimized LiMn[y]Fe[1−y]PO[4] as the Cathode for Lithium Batteries, Journal of The Electrochemical Society, **149**(6), 2002, A743 DOI: 10.1149/1.1473776.
4.HUANG, H., YIN, S.C., NAZAR, L.F., Approaching Theoretical Capacity of $LiFePO_4$ at Room Temperature at High Rates, Electrochemical and Solid-State Letters, **4**(10), 2001, A170 DOI: 10.1149/1.1396695.
5.KANG, B. ,CEDER, G., Battery materials for ultrafast charging and discharging, Nature, **458**(7235), 2009, 190-193 DOI: 10.1038/nature07853.
6.KWON, N.-H., DREZEN, T., EXNAR, I., TEERLINCK, I., ISONO, M., GRAETZEL, M., Enhanced Electrochemical Performance of Mesoparticulate $LiMnPO_4$ for Lithium Ion Batteries, Electrochemical and Solid-State Letters, **9**(6), 2006, A277 DOI: 10.1149/1.2191432.
7.YAMADA, A. ,CHUNG, S.-C., Crystal Chemistry of the Olivine-Type Li(Mn[y]Fe[1−y])PO[4] and (Mn[y]Fe[1−y])PO[4] as Possible 4 V Cathode Materials for Lithium Batteries, Journal of The Electrochemical Society, **148**(8), 2001, A960 DOI: 10.1149/1.1385377.
8.YAMADA, A., KUDO, Y., LIU, K.-Y., Phase Diagram of Li[x](Mn[y]Fe[1−y])PO[4] ($0 \leq x, y \leq 1$), Journal of The Electrochemical Society, **148**(10), 2001, A1153 DOI: 10.1149/1.1401083.
9.ZHOU, X., DENG, Y., WAN, L., QIN, X., CHEN, G., A surfactant-assisted synthesis route for scalable preparation of high performance of $LiFe_{0.15}Mn_{0.85}PO_4/C$ cathode using bimetallic precursor, Journal of Power Sources, **265**, 2014, 223-230 DOI: https://doi.org/10.1016/j.jpowsour.2014.04.049.
10.TOPRAKCI, O., TOPRAKCI, H.A.K., JI, L., ZHANG, X., Fabrication and Electrochemical Characteristics of $LiFePO_4$ Powders for Lithium-Ion Batteries, KONA Powder and Particle Journal, **28**, 2010, 50-73 DOI: 10.14356/kona.2010008.
11.MELIGRANA, G., DI LUPO, F., FERRARI, S., DESTRO, M., BODOARDO, S., GARINO, N., GERBALDI, C., Surfactant-assisted mild hydrothermal synthesis to nanostructured mixed ortho-

phosphates LiMnyFe1−yPO4/C lithium insertion cathode materials, Electrochimica Acta, **105**, 2013, 99-109 DOI: https://doi.org/10.1016/j.electacta.2013.04.153.
12.WANG, H., YANG, Y., LIANG, Y., CUI, L.-F., SANCHEZ CASALONGUE, H., LI, Y., HONG, G., CUI, Y., DAI, H., $LiMn_{1-x}F_{ex}PO_4$ Nanorods Grown on Graphene Sheets for Ultrahigh-Rate-Performance Lithium Ion Batteries, Angewandte Chemie International Edition, **50**(32), 2011, 7364-7368 DOI: 10.1002/anie.201103163.
13.HU, L., QIU, B., XIA, Y., QIN, Z., QIN, L., ZHOU, X., LIU, Z., Solvothermal synthesis of Fe-doping LiMnPO4 nanomaterials for Li-ion batteries, Journal of Power Sources, **248**, 2014, 246-252 DOI: https://doi.org/10.1016/j.jpowsour.2013.09.048.
14.CALIN, M., KHENOUSSI, N., SCHACHER, L., ADOLPHE, D., MANEA, L., GRADINARU, I., ZETU, I., STRATULAT, S., Morphological and Broadband Dielectric Spectroscopy Approaches on PA6 - CNT Nanofibres, *Mater. Plas*t., **50**(4), 2013, 257-263.
15.OBRADOVIC, V., STOJANOVIC, D., KOJOVIC, A., ZIVKOVIC, I., RADOJEVIC, V., USKOKOVIC, P., ALEKSIC, R., Electrospun Poly(vinylbutyral)/silica Composite Fibres for Impregnation of Aramid Fabrics, *Mater. Plast.*, **51**(3), 2014, 319-322.
16.HAGHI, A., KANAFCHIAN, M., KANAFCHIAN, M., Chitosan Electrospun Nanofibers Web, *Mater. Plast*., **49**(4), 2012, 253-259.
17.VON HAGEN, R., LORRMANN, H., MÖLLER, K.-C., MATHUR, S., Electrospun $LiFe_{1-y}Mn_yPO_4$/C Nanofiber Composites as Self-Supporting Cathodes in Li-Ion Batteries, Advanced Energy Materials, **2**(5), 2012, 553-559 DOI: 10.1002/aenm.201100534.
18.ZHANG, X., JI, L., TOPRAKCI, O., LIANG, Y., ALCOUTLABI, M., Electrospun Nanofiber-Based Anodes, Cathodes, and Separators for Advanced Lithium-Ion Batteries, Polymer Reviews, **51**(3), 2011, 239-264 DOI: 10.1080/15583724.2011.593390.
19.JI, L., TOPRAKCI, O., ALCOUTLABI, M., YAO, Y., LI, Y., ZHANG, S., GUO, B., LIN, Z., ZHANG, X., α-Fe2O3 Nanoparticle-Loaded Carbon Nanofibers as Stable and High-Capacity Anodes for Rechargeable Lithium-Ion Batteries, ACS Applied Materials & Interfaces, **4**(5), 2012, 2672-2679 DOI: 10.1021/am300333s.
20.XUE, L., FU, K., LI, Y., XU, G., LU, Y., ZHANG, S., TOPRAKCI, O., ZHANG, X., Si/C composite nanofibers with stable electric conductive network for use as durable lithium-ion battery anode, Nano Energy, **2**(3), 2013, 361-367 DOI: https://doi.org/10.1016/j.nanoen.2012.11.001.
21.BONINO, C.A., JI, L., LIN, Z., TOPRAKCI, O., ZHANG, X., KHAN, S.A., Electrospun Carbon-Tin Oxide Composite Nanofibers for Use as Lithium Ion Battery Anodes, ACS Applied Materials & Interfaces, **3**(7), 2011, 2534-2542 DOI: 10.1021/am2004015.
22.TOPRAKCI, O., JI, L., LIN, Z., TOPRAKCI, H.A.K., ZHANG, X., Fabrication and electrochemical characteristics of electrospun $LiFePO_4$/carbon composite fibers for lithium-ion batteries, Journal of Power Sources, **196**(18), 2011, 7692-7699 DOI: https://doi.org/10.1016/j.jpowsour.2011.04.031.
23.ZHANG, S., LIN, Z., JI, L., LI, Y., XU, G., XUE, L., LI, S., LU, Y., TOPRAKCI, O., ZHANG, X., Cr-doped Li_2MnSiO_4/carbon composite nanofibers as high-energy cathodes for Li-ion batteries, Journal of Materials Chemistry, **22**(29), 2012, 14661-14666 DOI: 10.1039/C2JM32213G.
24.TOPRAKCI, O., TOPRAKCI, H.A.K., JI, L., LIN, Z., GU, R., ZHANG, X., $LiFePO_4$ nanoparticles encapsulated in graphene-containing carbon nanofibers for use as energy storage materials, Journal of Renewable and Sustainable Energy, **4**(1), 2012, 013121 DOI: 10.1063/1.3690936.
25.TOPRAKCI, O., TOPRAKCI, H.A.K., JI, L., XU, G., LIN, Z., ZHANG, X., Carbon Nanotube-Loaded Electrospun $LiFePO_4$/Carbon Composite Nanofibers As Stable and Binder-Free Cathodes for Rechargeable Lithium-Ion Batteries, ACS Applied Materials & Interfaces, **4**(3), 2012, 1273-1280 DOI: 10.1021/am201527r.
26.LIU, X., QIN, X., WANG, X., LI, X., CHEN, S., Synthesis and performance of $LiFe_xMn_{1-x}PO_4$/C as cathode material for lithium ion batteries, Journal of Wuhan University of Technology-Mater. Sci. Ed., **30**(4), 2015, 655-659 DOI: 10.1007/s11595-015-1206-6.
Manuscript received: 1.03.2021